Journal Name

ARTICLE TYPE

Cite this: DOI: 10.1039/xxxxxxxxxx

On-surface synthesis of superlattice arrays of ultra-long graphene nanoribbons†

Cesar Moreno,*[a], Markos Paradinas[a], Manuel Vilas-Varela,[b‡], Mirko Panighel[a§], Gustavo Ceballos[a], Diego Peña[b] and Aitor Mugarza*[a,c†]

Received Date
Accepted Date

DOI: 10.1039/xxxxxxxxxx

www.rsc.org/journalname

We report the on surface synthesis of graphene nanoribbon superlattice arrays directed by the herringbone reconstruction of the Au(111) surface. The uniaxial anisotropy of the zigzag pattern of the reconstruction defines a one dimensional grid for directing the Ullmann polymerization and inducing periodic arrays of parallel ultra-long nanoribbons (>100 nm), where the periodicity is varied with coverage at discrete values following a hierarchical templating behavior.

One of the biggest advantage of on-surface synthesis with respect to top-down approaches lies on the capability to realize atomically precise nanostructures. A clear example of the power of this method is the synthesis of graphene nanoribbons (GNR) of perfect crystallinity, complex edge structures and controlled functionalization achieved since the seminal work of Cai and coworkers.[1,2] However, despite the formidable effort dedicated to structural engineering, very few studies focus on the control of their length[3] and spatial distribution on the surface.[4–7] These factors, being the main weakness of on-surface synthesis as compared to nanofabrication techniques, are in the same time crucial for the application of GNRs in devices. Indeed, the parallel alignment of long nanoribbons, and in particular the realization of superlattices with tunable spacings are of great interest for electronic and optolectronic applications.[8–12] The only strategy to syntesize GNR superlattices studied so far relies on the use of the stepped surfaces.[4,5,7] Here, periodically distributed monoatomic steps act as hard walls that direct the synthesis by impeding diffusion across adjacent terraces. However, this hard wall limitation also hinders the growth by reducing diffusion to one dimension, and inhibits interribon interactions that can drive superlattice structures, as the nanoporous graphene that we recently synthesized by the laterall covalent coupling of GNRs.[13]. By using the same home-designed precursor, $10,10'-$dibromo$-2,2'-$diphenyl$-9,9'-$bianthracene (DP-DBBA, Fig. 1a), we now report the capability of forming superlattices of decoupled GNRs of exceptional length that goes up to 200 nm, where the pitch can be tuned into different discrete values that range from 2 to 8 nm. We achieve that by combining efficient 2D diffusion over Au(111) terraces with the soft and hierarchical templating role of the herringbone reconstruction. The size of GNRs and superlattices are ultimately limited by the size of the zig-zag herringbone domains.

Our template is the $(22 \times \sqrt{3})$ herringbone reconstruction of the Au(111) surface, which consists on a periodic array of face-centred-cubic (fcc) and hexagonal-close-packed (hcp) stacking stripe domains separated by ridges where atoms fall out of registry.[14,15] Scanning tunneling microscopy (STM) can easily resolve such ridges as bright stripes, as can be seen in Fig. 1b. The zig-zag, herringbone pattern of the stripes reflects the alternating arrangement of 120° rotated domains that results from long-range interactions.[15,16] Interestingly one every two ridges, labelled as *x* in Fig. 1b, contains point dislocations that pinch in or bulge out the ridge boundaries at alternate elbows. The resulting 2D network of dislocations act as pinning and nucleation sites due to the lower coordination around the defect, and can enable the self-organization of 1D and 2D periodicic arrays of organic and inorganic nanostructures.[17–20]

The GNR precursor DP-DBBA (Fig. 1a) was sublimated onto the reconstructed surface of a Au(111) single crystal under ultra-high vacuum conditions and with the sample kept at room tem-

[a] *Catalan Institute of Nanoscience and Nanotechnology (ICN2), CSIC and The Barcelona Institute of Science and Technology, Campus UAB, Bellaterra, 08193 Barcelona, Spain; E-mail: cesar.moreno@icn2.cat*

[b] *Centro de Investigación en Química Biolóxica e Materiais Moleculares (CIQUS), Departamento de Química Orgánica, Universidade de Santiago de Compostela. 15782, Santiago de Compostela , Spain.*

[c] *ICREA-Institució Catalana de Recerca i Estudis Avançats, Lluis Companys 23, 08010 Barcelona, Spain*

† Electronic Supplementary Information (ESI) available: Coverage-dependent characterization of molecular precursors and GNR pinning at elbow sites. See DOI: 10.1039/b000000x/

‡ Present address:GalChimia, 15823 O Pino, Spain

§ Present address:CNR-IOM, S.S. 14 km 163.5, Basovizza, 34149 Trieste, Italy

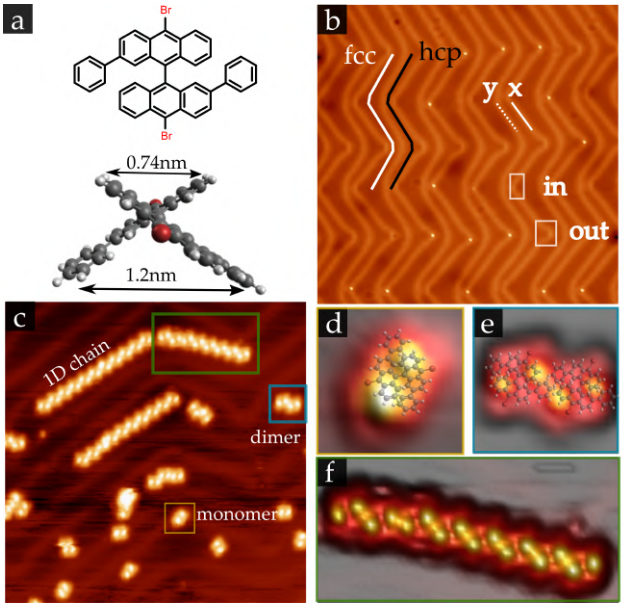

Fig. 1 Adsorption of monomers on Au(111). (a), Structural details of the precursor monomer DP-DBBA. The side view structure is relaxed in gas phase, with color labels: bromine, red; carbon, gray; hydrogen, white. **(b)**, Herringbone reconstruction of the pristine Au(111) surface; white boxes mark pinch-in and bulge-out dislocation sites (100x100 nm^2, I_t=0.3nA, V_s=0.2V). **(c)** STM image of as-sublimated DP-DBBA monomers (30x30 nm^2, I_t=0.1nA, V_s=1V). Close-up images of **(d)** an isolated monomer, **(e)** a dimer, and **(f)** a self-assembled molecular chain.

perature. Figure 1c shows an STM image acquired after cooling down the sample to 5 K, comprising intact, non-activated monomers. Similar to many other molecules,[20,21] DP-DBBA monomers preferentially adsorb within the most favorable fcc domains forming self-assembled 1D chains. Individual molecules are also trapped at the more reactive elbow sites, marked with a yellow square in Fig. 1c (see also Fig. S1 in ESI). The 0.74 nm distance between the double protrusions imaged by STM agrees nicely with the high-end benzene rings of the staggered anthracene pair, considerably shorter than the 1.2 nm spacing between the phenyl substituents (Fig. 1a). Based on that, we can conclude that molecules adsorb with the phenyl substituents pointing towards the surface as depicted in Fig. 1d. This phenyl-driven molecule-surface interaction in DP-DBBA, different from the anthracene-driven one in DBBA, may play a principal role in the very distinct growth behavior we describe in the following.

Annealing the sample at $T \sim 200\,^{\circ}$C induces Ullmann polymerization. Figure 2a shows a close look of the resulting polymeric chains, observed as a sequence of protrusion pairs that correspond to monomer units, with a period of 0.84 nm that is consistent with the inter-monomer spacing of other DBBA-based polymers[1]. The polymeric chains assemble in bundles, very likely due to the π-stacking interactions between the staggered anthracenes.[22] In contrast to all previous studies of GNR synthesis, the chains are all aligned along the zig-zag direction of the herringbone reconstruction (Figs. 2b,c). We note that this orientation is not compatible with the previous self-assembly of the precursors at room temperature, which form multiple rotational domains (see Fig. S1 in ESI for more details). The well-defined direction of the chains, correlated with the reconstruction but not following the preferential fcc domain direction, can only be explained if the growth is directed by the elbow sites, disregarding any templating effect of the zig-zag arrangement of the stacking domains. Indeed, a close look at individual bundles reveals the pinning of peripheral chains at elbow sites (circles in Fig. 2b), which seems to direct the growth of the rest of the bundle. This growth process can lead to extraordinarily long 1D polymeric chains in excess of 100 nm (Fig. 2c), which we attribute to three factors: the parallel growth of adjacent chains, which avoids crossing each other; an efficient diffusion, very likely related to the phenyl-driven interaction with the surface; a large thermal energy window that separates Ullmann coupling from cyclodehydrogenation, keeping the growth process free of excess H that could block the polymerization by capping the termination C radicals.[3]

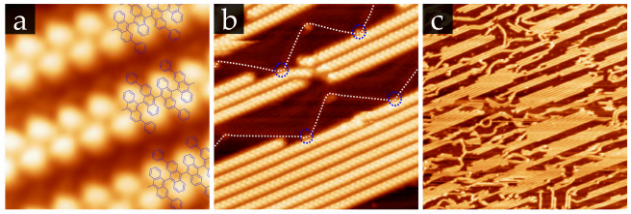

Fig. 2 Ultra-long 1D polymeric chains. (a) Close-up STM image, 4.4x4.4 nm^2, displaying three self-assembled polymeric chains observed as a sequence of pairs of bright protrusions. **(b)** Medium-scale STM image, 28x28 nm^2, showing the directional growth of polymeric chains along the zigzag orientation of the herringbone reconstruction. The *x* ridges are marked with dotted white lines, and the pinning elbow sites with dotted blue circles. **(c)** Large-scale STM image, 140x140 nm^2, showing the long-range ordered alignment and the lateral assembly of the polymeric chains into bundles. Polymeric chains up to 150 nm length are observed. Scanning parameters: I_t=0.1nA, V_s=1.2V.

Further annealing at $T \sim 400\,^{\circ}$C promotes planarization via cyclodehydrogenation[1,13], converting the staggered polymers into planar GNRs. Figure 3a displays a high resolution STM image of an isolated GNR, obtained with a CO-functionalized tip.[23] The periodic arrangment of bays separated by the fused phenyl substituents can also be seen as series of consecutive pairs of 7 and 13 C atom wide chains, and hence we label the ribbon 7-13-GNR. This particular edge structure is responsible of the low band gap of 1.0 eV found for this GNR, and represents a superlattice potential for electrons dispersing along the ribbon.[13] Zooming out to study the distribution of ribbons, we can see in Figs. 3b-d that they preserve the preferential alignment along the zig-zag direction (see also Fig. 4), but are now debundled into individual chains, consistent with the increased ribbon-substrate to interribbon interaction ratio expected after the planarization of the chain.[22] Isolated GNRs in excess of 100 nm can be routinely obtained, eventually reaching record values up to 200 nm (Fig. 3b).

A statistical analysis over mesoscopic areas result in average lengths around 70 nm (Fig. 3d), however the spatial distribution is not random, shorter GNRs being mainly located at regions where the zig-zag herringbone pattern is small or not well-

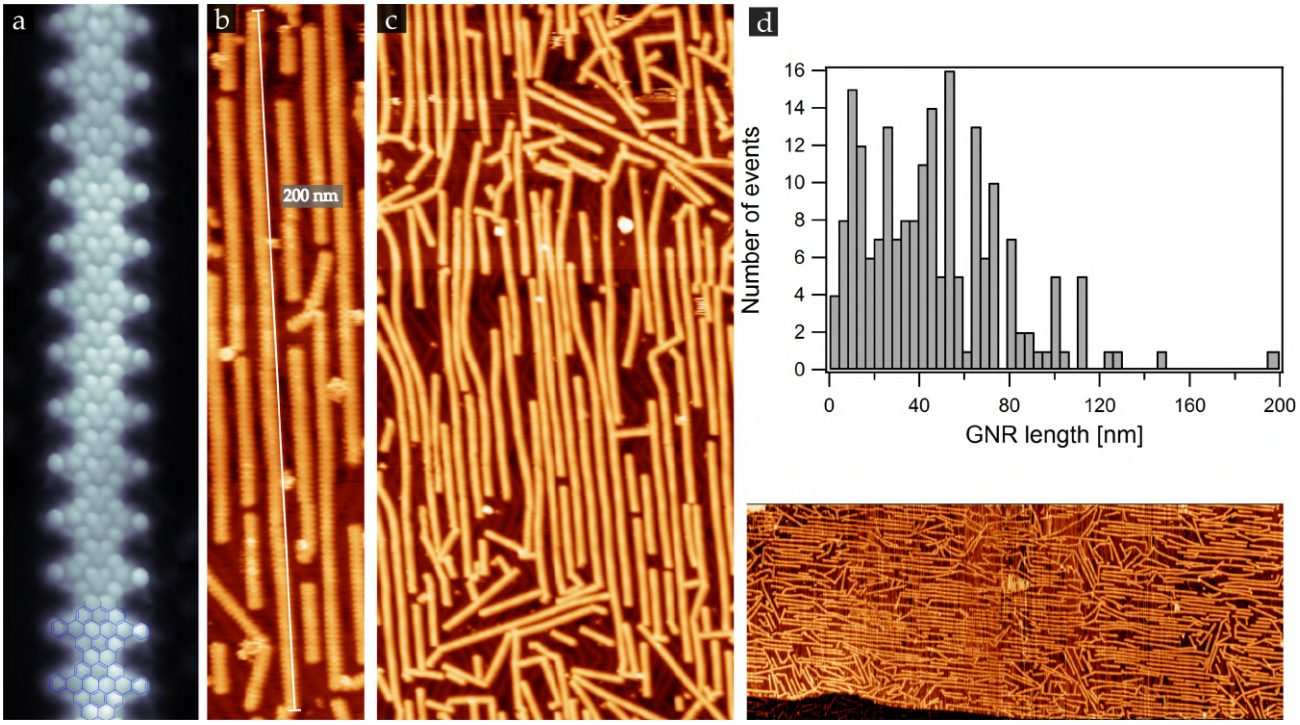

Fig. 3 Ultra-long graphene nanoribbons. **(a)** High resolution STM image of a single GNR resolved with a CO-tip (6x22 nm^2, I_t=0.02nA, V_s=1V). **(b)** Ultra-long, parallel GNRs with lengths up to 200 nm (60x203 nm^2, I_t=0.1nA, V_s=1.5V). **(c)** STM image overview displaying a high density array of parallel GNRs (100x200 nm^2, I_t=0.05nA, V_s=1V). **(d)** Length-distribution histogram compiled from the large-scale STM image displayed at the bottom (200x500 nm^2, I_t=0.02nA, V_s=1V).

defined, and large herringbone domains containing GNRs with average values closer to 100 nm. In any case, this average length is significantly larger than previously reported values for different types of GNRs, ranging from 23-45 nm.[1,3–5]

The templating role of the herringbone reconstruction is not limited to direct the growth direction, but it also imprints its periodicity, providing the two ingredients required for the formation of superlattices. From the STM images of Fig. 3 one can indeed perceive a certain order in the interribbon spacing. A more systematic coverage-dependent study unveils a hierarchical templating mechanism that enables the fabrication of superlattices of different periodicities.

Figure 4a shows an image of a diluted distribution of GNRs. The single mode periodicity of the array is clearly seen by the sharp dots in the Fourier transform of the image (inset), that translate in a period of 7.8 nm. This value is very close to the 7.3 nm that corresponds to the periodicity of a single type of elbow dislocations in the direction perpendicular to the zig-zag (see top sketch). By looking close to individual GNRs, we notice that these are not pinned to elbow dislocations, but are instead confined between two continuous, dislocationless *y* ridges, as shown in Fig. 4a (see Fig. S2 in ESI for more details). We attribute this shift of preferential site to the stronger π interaction of the planar backbone of the GNR with the substrate, which tends to maximize the contact area with the fcc domains, and minimize the crossing over ridges in this new configuration.

Interestingly, this preferential pinning mechanism opens the opportunity for a hierarchical use of the herringbone template by tuning the coverage. Beyond the saturation of the new preferential sites at ~0.25 ML, additional GNRs occupy the elbow sites at intermediate distances, giving rise to a a new periodicity of 3.8 nm (Fig. 4b). Finally, beyond 0.50 ML additional GNRs start to cover the interstitial regions, which at the saturation coverage results in a periodicity of 1.9 nm (Fig. 4c). At this coverage interribon steric forces might dominate lateral interactions.

In summary, we report on the use of the reconstructed Au(111) surface as a catalytic nanostructured template for the on-surface synthesis of superlattices of atomically precise GNRs. The molecule-substrate interaction is weak enough to overcome the preferential fcc domain boundaries and use the rectangular network of elbow dislocations to direct the growth during the polymerization step. This directed growth enables the synthesis of polymer chains (and subsequently GNRs) of exceptional lengths as compared to previous on-surface synthesis studies. Planarization of the polymer chains into GNR increases the substrate-interchain interaction. This leads to a debunching of the chains into individual GNRs that are positioned at preferential sites that maximize contact with fcc domains, and consequently to the formation of a one dimensional superlattice of GNRs. The periodicity of the superlattice can be varied into three discrete values by controlling the coverage thanks to the hierarchical templating behavior of the surface reconstruction. The realization of parallel arrays of ultra-long GNRs can be crucial to improve the performance of field-effect transistors by increasing the channel length and providing multichannel components that withhold higher current thresholds. On the other hand, the lateral order can be exploited

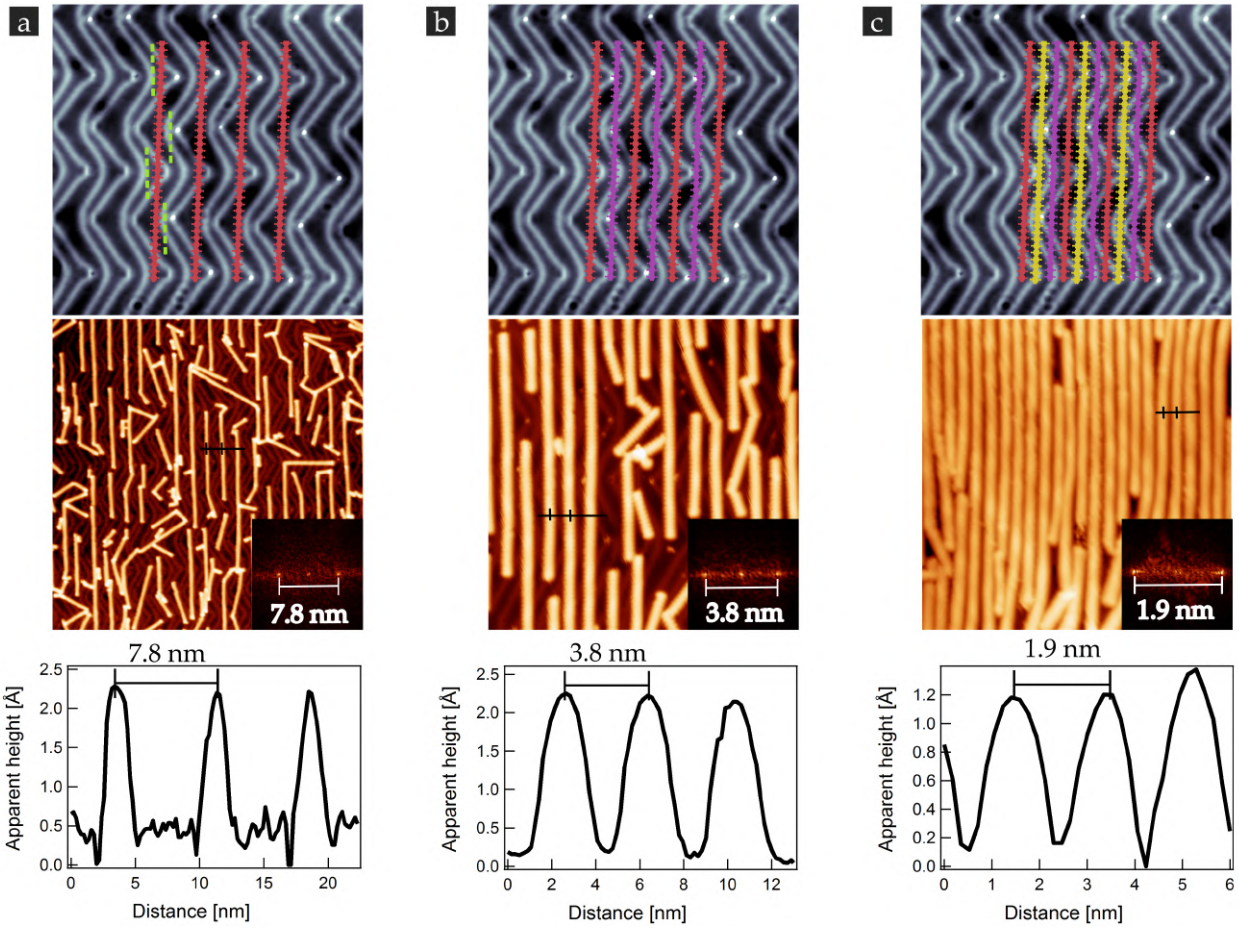

Fig. 4 Hierarchical surface-guided ordering of graphene nanoribbons. (a-c) STM images of the periodic arrangement of GNRs as a function of coverage, with increasing coverage from **(a)** to **(c)**. The top images are sketched GNRs represented on top of a herringbone pattern. Dots indicate bulge-out (yellow) and pinch-in (green) dislocation sites. The center images show the GNR superlattices. Their periodicity is revealed by the Fourier transform of the images (inset), and real space profiles (bottom graphs). Scanning parameters are: **(a)** (150x150 nm^2, I_t=0.07nA, V_s=0.5V); **(b)** (60x60 nm^2, I_t=0.06nA, V_s=0.1V); **(c)** (40x40 nm^2, I_t=0.4nA, V_s=1.2V).

in coupled devices, such as optical superlattices.

C.M was supported by the Agency for Management of University and Research grants (AGAUR) of the Catalan government through the FP7 framework program of the European Commission under Marie Curie COFUND action 600385. M.P. thanks the Spanish Government for financial support through PTA2014-09788-I. Funded by the CERCA Programme / Generalitat de Catalunya. ICN2 is supported by the Severo Ochoa program from Spanish MINECO (Grant No. SEV-2013-0295). We acknowledge support from the Ministerio de Ciencia e Innovación (MAT2013-46593-C6-2-P, MAT2013-46593-C6-5-P, MAT2016-78293-C6-2-R, MAT2016-78293-C6-4-R, and Severo Ochoa no. SEV-2013-0295), the EU project PAMS (610446) the Xunta de Galicia (Centro singular de investigacion de Galicia accreditation 2016-2019, ED431G/09), and the European Regional Development Fund.

Conflicts of interest

There are no conflicts to declare.

Notes and references

1 J. Cai, P. Ruffieux, R. Jaafar, M. Bieri, T. Braun, S. Blankenburg, M. Muoth, A. P. Seitsonen, M. Saleh, X. Feng, K. Mullen and R. Fasel, *Nature*, 2010, **466**, 470–473.
2 L. Talirz, P. Ruffieux and R. Fasel, *Advanced Materials*, 2016, **28**, 6222–6231.
3 M. Di Giovannantonio, O. Deniz, J. I. Urgel, R. Widmer, T. Dienel, S. Stolz, C. Sánchez-Sánchez, M. Muntwiler, T. Dumslaff, R. Berger, A. Narita, X. Feng, K. Müllen, P. Ruffieux and R. Fasel, *ACS Nano*, 2018, **12**, 74–81.
4 S. Linden, D. Zhong, A. Timmer, N. Aghdassi, J. H. Franke, H. Zhang, X. Feng, K. Müllen, H. Fuchs, L. Chi and H. Zacharias, *Phys. Rev. Lett.*, 2012, **108**, 216801.
5 D. G. de Oteyza, A. Garcia-Lekue, M. Vilas-Varela, N. Merino-Díez, E. Carbonell-Sanromà, M. Corso, G. Vasseur, C. Rogero, E. Guitián, J. I. Pascual, J. E. Ortega, Y. Wakayama and D. Peña, *ACS Nano*, 2016, **10**, 9000–9008.
6 J. D. Teeter, P. S. Costa, M. Mehdi Pour, D. P. Miller, E. Zurek, A. Enders and A. Sinitskii, *Chem. Commun.*, 2017, **53**, 8463–8466.
7 N. Merino-Díez, J. Lobo-Checa, P. Nita, A. Garcia-Lekue, A. Basagni, G. Vasseur, F. Tiso, F. Sedona, P. K. Das, J. Fujii, I. Vobornik, M. Sambi, J. I. Pascual, J. E. Ortega and D. G. de Oteyza, *J. Phys. Chem. Lett.*, 2018, **9**, 2510–2517.
8 X. Liang and S. Wi, *ACS Nano*, 2012, **6**, 9700–9710.
9 H. Suzuki, T. Kaneko, Y. Shibuta, M. Ohno, Y. Maekawa and T. Kato, *Nature Communications*, 2016, **7**, 11797.
10 J. G. Son, M. Son, K. J. Moon, B. H. Lee, J. M. Myoung, M. S. Strano, M. H. Ham and C. A. Ross, *Advanced Materials*, 2013, **25**, 4723–4728.
11 A. Y. Nikitin, F. Guinea, F. J. Garcia-Vidal and L. Martin-Moreno, *Physical Review B - Condensed Matter and Materials Physics*, 2012, **85**, 1–4.
12 I. Silveiro, J. M. P. Ortega and F. J. G. de Abajo, *Light: Science & Applications*, 2015, **4**, e241.
13 C. Moreno, M. Vilas-Varela, B. Kretz, A. Garcia-Lekue, M. V. Costache, M. Paradinas, M. Panighel, G. Ceballos, S. O. Valenzuela, D. Peña and A. Mugarza, *Science*, 2018, **360**, 199.
14 C. Wöll, S. Chiang, R. J. Wilson and P. H. Lippel, *Phys. Rev. B*, 1989, **39**, 7988–7991.
15 J. V. Barth, H. Brune, G. Ertl and R. J. Behm, *Phys. Rev. B*, 1990, **42**, 9307–9318.

16 S. Narasimhan and D. Vanderbilt, *Physical Review Letters*, 1992, **69**, 1564–1567.
17 D. D. Chambliss, R. J. Wilson and S. Chiang, *Phys. Rev. Lett.*, 1991, **66**, 1721–1724.
18 B. Voigtländer, G. Meyer and N. M. Amer, *Phys. Rev. B*, 1991, **44**, 10354–10357.
19 N. Weiss, T. Cren, M. Epple, S. Rusponi, G. Baudot, S. Rohart, A. Tejeda, V. Repain, S. Rousset, P. Ohresser, F. Scheurer, P. Bencok and H. Brune, *Physical Review Letters*, 2005, **95**, 1–4.
20 D. Écija, R. Otero, L. Sánchez, J. M. Gallego, Y. Wang, M. Alcamí, F. Martín, N. Martín and R. Miranda, *Angewandte Chemie International Edition*, 2007, **46**, 7874–7877.
21 Z. H. Cheng, L. Gao, Z. T. Deng, Q. Liu, N. Jiang, X. Lin, X. B. He, S. X. Du and H.-J. Gao, *The Journal of Physical Chemistry C*, 2007, **111**, 2656–2660.
22 C. Bronner, T. Marangoni, D. J. Rizzo, R. A. Durr, J. H. Jørgensen, F. R. Fischer and M. F. Crommie, *J. Phys. Chem. C*, 2017, **121**, 18490–18495.
23 P. Hapala, G. Kichin, C. Wagner, F. S. Tautz, R. Temirov and P. Jelínek, *Phys. Rev. B*, 2014, **90**, 085421.